Aeolian sediment transport through large patches of roughness in the atmospheric inertial sublayer

John A. Gillies,[1] William G. Nickling,[2] and James King[2]

Received 2 November 2005; revised 13 February 2006; accepted 23 February 2006; published 4 May 2006.

[1] Roughness influences the flux of wind-driven sand transport. In this paper, we report on sediment transport measurements for four different surface roughness configurations composed of the same size (solid) roughness elements in the atmospheric inertial sublayer. Results of these tests indicate that sediment transport rates through patches of roughness in the atmospheric inertial sublayer are to a large extent controlled and scale proportionally with the roughness density ($\lambda = n\ b\ h/S$, where n is number of elements of breadth b and height h in area S) of the surface. However, element size apparently increases the magnitude of the reduction beyond that attributable to λ. A sediment transport model that incorporates the effect of shear stress partitioning appears to predict reasonably well the effect of roughness on sand transport in the cases where the roughness elements are $\leq$0.10 m in height. However, when the dimensions of the roughness itself are equivalent to or are greater than the range of saltation lengths (vertical and horizontal), additional interactions of the elements with the saltation cloud appear to reduce the transport efficiency.

Citation: Gillies, J. A., W. G. Nickling, and J. King (2006), Aeolian sediment transport through large patches of roughness in the atmospheric inertial sublayer, *J. Geophys. Res.*, *111*, F02006, doi:10.1029/2005JF000434.

1. Introduction

[2] The entrainment and transport of sediment by wind results from the horizontal shearing stress (τ) generated at the surface by boundary layer winds. If τ is of sufficient magnitude to overcome the inertial and bonding forces of the surface-bound particles they can be entrained and transported by the wind. Over a flat surface with no large roughness elements, the time-averaged τ is normally assumed to be relatively uniform and directly related to the wind profile characteristics. However, in the presence of roughness elements (pebbles to boulders or vegetation) the surface shearing stress is neither spatially nor temporally uniform because of the sheltering of the surface by the roughness elements and the generation of turbulent wakes that are shed from individual elements. In addition to the effect roughness can have on the modulation of shearing stress among the elements, the process is also affected by the interaction of the saltating particles with the roughness elements themselves [*Bagnold*, 1941; *McKenna Neuman and Nickling*, 1995].

[3] Understanding the controls of roughness on aeolian sediment transport has important ramifications for successfully predicting how it affects the entrainment and transport of sediment by wind on Earth. This is even more important for Mars because aeolian processes are affecting the evolution of the Martian surface to a much greater degree than they do on Earth [*Malin et al.*, 1998; *Wilson and Zimbelman*, 2004].

[4] In this paper, we report on sediment transport measurements for four different surface roughness configurations composed of the same size (solid) roughness elements in the atmospheric inertial sublayer (ISL). The ISL is defined as the region in the atmosphere where the logarithmic law applies.

[5] The rough surfaces constructed for this experiment are conceptualized as being large patches in which sediment transport may be initiated and through which sand may be transported by the wind. This situation of alternating patches of smooth and roughened surfaces over or through which wind blown sand is transported is often observed in terrestrial deserts and on the surface of Mars (see for example, http://marsrovers.jpl.nasa.gov/home/).

[6] Although the transport of sand by wind has been investigated in wind tunnel experiments [e.g., *Lyles et al.*, 1974; *Logie*, 1981; *Buckley*, 1987; *Gillette and Stockton*, 1989; *McKenna Neuman and Nickling*, 1995; *Nickling and McKenna Neuman*, 1995; *Al-Awadhi and Willetts*, 1999] there are some concerns over scaling issues (e.g., element heights, saltation path lengths, and maximum trajectory heights) that may limit the direct comparison of wind tunnel tests to field situations. *White and Mounla* [1991] discuss how wind tunnels, due to Froude number effects, can constrain the saltation system. In addition to these effects, differences between the size of the elements and cross-sectional area of a wind tunnel can enforce a height limit on the elements due to flow blocking and the creation of adverse pressure gradients.

[1] Particle Emissions Measurement Laboratory, Division of Atmospheric Sciences, Desert Research Institute, Reno, Nevada, USA.
[2] Wind Erosion Laboratory, Department of Geography, University of Guelph, Guelph, Ontario, Canada.

0148-0227/06/2005JF000434

[7] Field studies [e.g., *Greeley et al.*, 1995; *Lancaster and Baas*, 1998] of sand transport in the presence of roughness have been limited. Previously in field experiments there has been limited control on the range of roughness tested and there was a reliance on preexisting roughness, which makes sampling over many different surfaces logistically difficult and the development of general relationships problematic. In our study the amount and size of the roughness was strictly controlled. A unique aspect of this field study is that the size of the roughness elements is approximately an order of magnitude larger than elements that have been used in wind tunnel experiments to examine the effect of roughness on aeolian transport of sand. In addition, because our study was conducted in a field setting there were no constraints on the saltation system, the boundary layer flow, or the size of the roughness elements that were used.

[8] The study presented in this paper describes the effect that large solid roughness elements arranged in varying roughness densities have on the transport of sediment by wind in a field situation. Sediment transport rates in front of and within different arrays of staggered roughness elements were measured with active sediment traps, which collect sand entering into them through a vertical slot and Safire piezoelectric saltation sensors [*Baas*, 2004], which monitor saltation activity. In addition, the total shear stress (τ) in the ISL, the shear stress on the intervening surface (τ_S), and the force of drag on the elements were measured simultaneously, along with the sediment transport measurements. The measurement of τ, τ_S, and drag on the elements were accomplished with measurements of the vertical wind speed profile using anemometers, skin friction meters (Irwin sensors), and drag balances, respectively. The roughness configurations were also under strict control in this experiment as they were constructed to fairly rigorous dimensional standards.

[9] It is important to note that in this study, the roughness elements were positioned on a relatively hard, supply limited surface that for the most part did not supply grains to the air stream during the transport events. Rather, sand transported through the system was almost totally derived from small dunes upwind of the element array. As a result, grains moving through the array were transported in saltation (high-energy transport) with few grains being ejected and transported in reptation (low-energy transport). This differs from transport on a sand sheet where a large proportion of the sediment flux consists of reptation driven by saltation impacts. Results of our field experiments suggest that this difference does not result in a significant difference in the pattern of transport and distribution of stresses.

2. Background

[10] Nonerodible roughness elements whether by virtue of their size, as in the case of pebbles, cobbles, or boulders, or by virtue of their being anchored in the soil (e.g., vegetation), reduce sediment loss by wind in four ways: (1) roughness elements shelter the surface by covering a portion of it, (2) the presence of a sufficient number of them will reduce the shear stress in the intervening area by extracting momentum from the wind at a height above the surface, (3) they provide, in the case of solid and porous elements a zone of reduced shear stress in their lee and in addition porous elements such as vegetation can trap particles within their structure, and (4) the presence of nonerodible elements can effect the number and efficiency of grain/bed collisions.

[11] The role of roughness elements in the reduction of shearing stress on the intervening surface among roughness elements and its effect on the threshold of entrainment has been an important area of research for increasing knowledge of aeolian sediment transport processes [e.g., *Wooding et al.*, 1973; *Gillette and Stockton*, 1989; *Raupach et al.*, 1993]. Shear stress partitioning theory [*Schlichting*, 1936] has proved to be a useful framework in which to evaluate roughness effects on sediment transport processes. The theory states simply that as roughness increases, τ increases, but a greater percentage of the stress is taken up by the nonerodible elements leaving less stress on the intervening surface (τ_s) to mobilize erodible particles. *Raupach* [1992] and *Raupach et al.* [1993] proposed a predictive physically based model for the partitioning of wind shear between solid elements having well-defined wakes and the intervening bare surface.

[12] The model allows the user to specify available inputs to describe most environments and generate the ratio that characterizes the erosion threshold of an initially bare erodible surface with the threshold once nonerodible elements are present. This relationship is expressed in terms of the threshold wind shear velocity ratio (R_t), that defines the ratio between the threshold wind shear velocity over a smooth surface and a similar surface covered with nonerodible roughness elements. This may be generalized further to the shear velocity ratio (R) that simply characterizes the ratio for simultaneous shear velocities (or shear stresses) of the bare soil and a rough surface, irrespective of threshold conditions. In this study, we determined R from measurements and consider it synonymous with R_t when comparing with data from other sources.

[13] The *Raupach et al.* [1993] model is expressed as:

$$R_t = \frac{u_{*tS}}{u_{*tR}} = \frac{1}{(1 - m\sigma\lambda)^{0.5}(1 + m\beta\lambda)^{0.5}} \tag{1}$$

where, u_{*tS} is threshold shear velocity of bare surface (m s^{-1}), u_{*tR} is threshold wind shear velocity with roughness elements (m s^{-1}), σ is the roughness element basal area to frontal area ratio, λ is roughness density, β is the ratio of element to surface drag coefficients, and m is an empirical constant ranging from 0 to 1 that accounts for the spatial heterogeneity of surface shear stress.

[14] The roughness density (λ) is defined as:

$$\lambda = n\ b\ h/S \tag{2}$$

where n is the number of roughness elements occupying the ground area S (m^2), b is element breadth (m), and h element height (m).

[15] Recent analysis by *King et al.* [2005] has shown that this model is very robust in its ability to predict R_t for a surface using appropriate input parameters and predicted values of R_t show good agreement with measured R_t values for both wind tunnel and field data. J. A. Gillies et al. (Shear

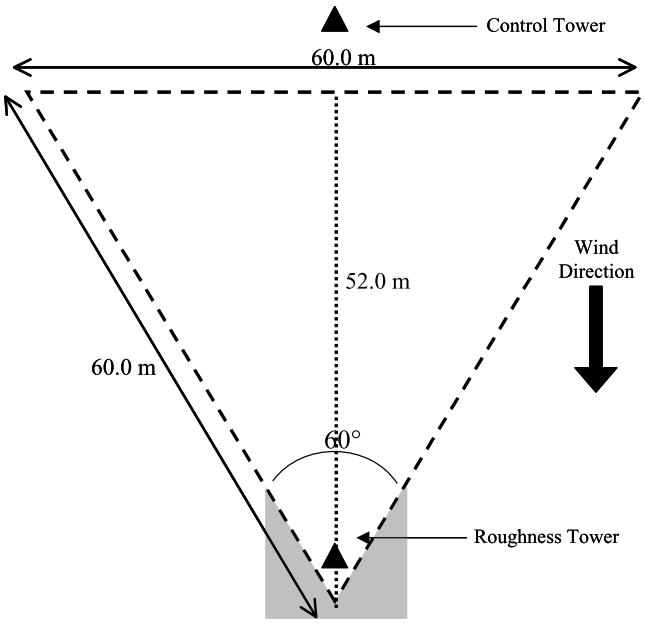

Figure 1. Dimensions of the roughness arrays shown in Figure 2. The shaded area is a region where extra roughness elements were placed around the downwind tower matching exactly the row and interelement spacing as the triangular roughness array, preserving the target λ.

stress partitioning in large patches of roughness in the atmospheric inertial sublayer, submitted to *Boundary-Layer Meteorology* 2005, hereinafter referred to as Gillies et al., submitted manuscript, 2005) have also demonstrated that the model can predict the shear stress partitioning in large patches of roughness in the ISL. *Orndorff* [1998] has suggested this model can also be applied to evaluate partitioning effects on sediment transport rates. In *Orndorff*'s [1998] model the transport of sediment is controlled by the link between τ and the horizontal saltation flux Q (kg m^{-1} s^{-1}) as initially theorized by *Bagnold* [1941], and subsequently demonstrated in numerous studies [e.g., *Anderson and Willetts*, 1991; *McEwan and Willetts*, 1994; *Sørensen*, 2004]. In *Orndorff*'s [1998] model, Q within the roughness scales with τ_S, which is predicted using *Raupach et al.*'s [1993] model (i.e., equation (1)). Several authors have suggested that under conditions where $\lambda \geq 0.5$ sediment transport by wind will not occur for the typical range of expected boundary layer shear stresses associated with the terrestrial ISL.

[16] Low-density arrays have been shown by *Logie* [1981] and others [e.g., *Nickling and McKenna Neuman*, 1995] to increase sediment transport rates. This increase is attributed to several factors: (1) a higher τ due to the increase in roughness, (2) the increase in the number of highly elastic collisions between saltating sand grains and the roughness elements, which promotes grain ejection and transport, and (3) an increase in localized shear stress above entrainment threshold associated with the generation of turbulent eddies from the roughness elements that frequently results in scour around the elements.

[17] In sufficient numbers, roughness will work to the detriment of sediment transport due to the interaction that affects the number and effectiveness of grain/bed collisions on the erodible surface. *Al-Sudairawi* [1992] in a wind tunnel study concluded that the nonerodible elements shelter a portion of the erodible surface preventing saltating grains from impacting and splashing up new grains. *Al-Awadhi and Willetts* [1999] also noted that this sheltering can be conceived as a shadow downwind of the nonerodible elements and is a function of the approach angle of the saltating grains (9–14°) and the aspect area of the elements.

3. Experimental Procedures

[18] In the spring of 2004 the sediment transport field experiment was established at the Jornada Experimental Range (JER) of the U.S. Department of Agriculture near Las Cruces, NM. A large barren area was selected within the JER known as the Scrape site [*Gillette and Chen*, 2001] (total area $\approx$ 10,000 m^2) in that it possessed several critical attributes. This particular site was of special interest because it provided: (1) an extensive bare surface area where a range of roughness configurations could be deployed without having to move locations, (2) an upwind fetch of $\approx$60 m of smooth surface for the prevailing wind direction before it would encounter a roughness array, (3) frequent wind of consistent direction, (4) an upwind coppice dune field that provided a source of sand, and (5) it provided a safe and secure environment for personnel and the scientific instruments at all times.

3.1. Roughness Arrays

[19] For this study five gallon plastic buckets (0.26 m $\times$ 0.30 m $\times$ 0.36 m) were used as the nonerodible roughness elements. Each bucket was filled with two shovel scoops of sand and the lid replaced in order to prevent it from moving or falling over during high winds. The form of a bucket is a slightly tapering cylinder, the projected frontal area form being an isosceles trapezoid. The buckets were placed on the surface with the wide end (i.e., lid end) down. These buckets were used to construct staggered arrays of roughness elements of varying λ. In calculating λ, the frontal area of the bucket (0.101 m^2) was used to represent the product of b multiplied by h (0.36 m) in equation (2). The roughness array was in the form of an equilateral triangle with 60-m-long sides and the long axis aligned with the expected dominant wind direction (Figure 1).

[20] The position of each element in the array was determined by carefully marking the location in a grid defined by the intersection of 1.6 mm (1/16th inch) diameter aircraft cable the ends of which were staked for each roughness array configuration to provide the proper interelement spacing to achieve the target λ values.

[21] The length dimensions, number of elements, and roughness densities of the test surfaces and positions of the instruments referenced from the front of the array are listed in Table 1. A roughness array was left in place until sufficient data were collected to characterize the aerodynamic properties of the surface, the shear stress partitioning associated with the array, and sediment transport had occurred. Images of the four roughness arrays are shown in Figure 2. Data were deemed acceptable for analysis only for winds that entered and exited the array 20° either side of the azimuth of the centerline of the array (215°). One

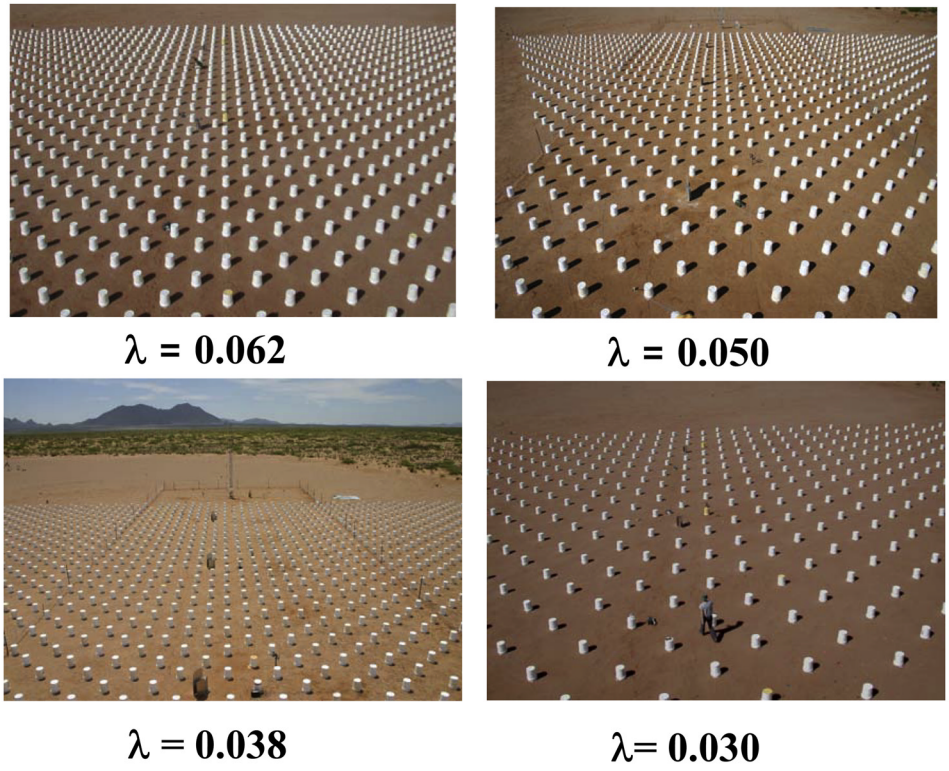

Figure 2. Images of the four roughness arrays used in the experiments.

exception was made for the data collected on 1 May 2004 where the average wind direction was 280° (±27°).

3.2. Total Shear Stress in the ISL, τ

[22] Vertical wind speed profiles were measured with arrays of 8 logarithmically spaced cup anemometers mounted on 1-m-long boom arms on two 9-m-high towers. The heights of the anemometers above the base of the tower were identical for both towers. One tower was located near the apex of the roughness array and the other was placed outside the array (i.e., upwind) to measure the wind speed profile over the bare surface that was unaffected by the roughness elements. Wind direction was also measured with vanes mounted on both anemometer towers at 9 m.

Table 1. Roughness Element Characteristics and Instrument Positions for the Four Roughness Arrays

Array Characteristics	λ = 0.062	λ = 0.050	λ = 0.038	λ = 0.030
Spacing of roughness elements (m) (center to center of bucket in the axial direction)	1.800	2.060	2.300	2.548
Number of roughness elements (not including buckets surrounding the array tower)	1111	900	681	533
Distance (m) from leading edge of roughness to:				
Irwin Sensor position 1	48.00	45.93	47.20	46.02
Irwin Sensor position 2	37.2	38.35	37.95	38.23
Drag Balance 1	35.2	36.2	36.85	34.80
Sediment Trap 1	37.00	38.25	39.00	37.27
Safire 1	39.00	40.35	41.50	40.09
Irwin Sensor position 3	30.00	29.77	31.05	30.25
Irwin Sensor position 4	22.45	21.65	21.85	22.65
Drag Balance 2	20.70	20.00	20.45	19.40
Sediment Trap 2	22.50	22.05	22.80	21.93
Safire 2	24.30	24.25	25.30	24.56
Irwin Sensor position 5	15.50	14.25	14.90	15.70
Irwin Sensor position 6	8.20	7.96	8.00	7.76
Drag Balance 3	6.25	6.02	6.45	6.30
Sediment Trap 3	8.00	7.85	9.00	8.91
Safire 3	10.00	10.20	11.45	11.58
Distance (m) in front of leading edge of roughness to:				
Control Instruments: Irwin Sensor	5.27	5.27	5.27	5.27
Sediment Trap 4, Safire 4	5.27	5.27	5.27	5.27

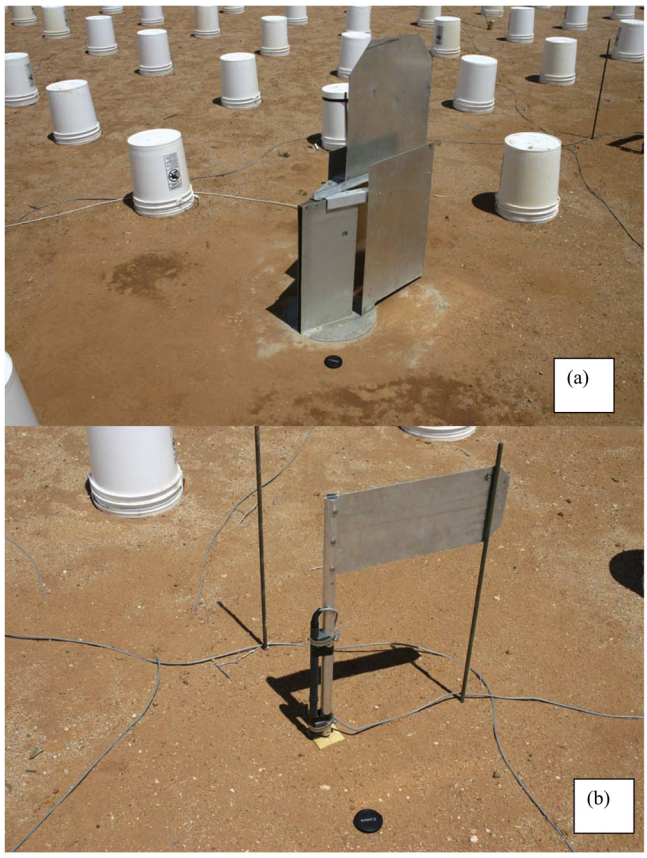

Figure 3. (a) Self-orienting sand trap used to measure saltation flux. A balance is located beneath the wedge-shaped slotted trap that receives the sand moving in saltation. (b) Piezoelectric Safire saltation sensor attached to a self-orienting vane.

[23] Shear velocity (u_*) was determined by fitting the 10-min average vertical wind speed data using least squares regression to the "law of the wall." The "law of the wall" describes the logarithmic wind speed profile observed in the ISL and is represented by the equation:

$$\frac{u_z}{u_*} = \frac{1}{\kappa} \ln\left(\frac{z}{z_o}\right) \tag{3}$$

where u_z (m s^{-1}) is mean wind speed at height z (m), κ is the von Kármán constant (0.4), and z_o is aerodynamic roughness length (m).

[24] Numerous studies show that when wind encounters and flows over a rough surface the wind profile may be displaced upward requiring the addition of a displacement height term (d) in the Prandtl-von Kármán equation (i.e., equation (3)). Unfortunately there are few guidelines in the literature as to when a displacement is required with regard to the height, width and distribution of the roughness elements. As noted by Gillies et al. (submitted manuscript), it was not possible to resolve a measure of d [*Jackson*, 1981] for these surface roughness configurations as the iterative procedure they used to estimate d did not result in an appreciable improvement in the fit of the 10-min average wind profiles to the "law of the wall" and in many instances produced values of d that did not make physical sense (i.e., d was negative).

[25] According to *MacDonald et al.* [1998] for the surfaces tested, d should range between ≈0.02 m for the least dense and ≈0.07 m for the most dense array. A value for d was not used in the calculation of u_* in this study. Estimates of the total shear stress (τ) were determined for both towers using the relationship:

$$\tau = \rho_a u_*^2 \tag{4}$$

where ρ_a is air density (kg m^{-3}).

3.3. Surface Shear Stress, τ_S, and Element Drag Force

[26] Shear stress on the surface within an array was measured with Irwin sensors. The Irwin sensor is a simple, omni-directional skin friction meter that measures the near surface vertical pressure gradient [*Irwin*, 1980]. Once calibrated, the Irwin sensor can be used to measure surface shear stress at frequencies greater than 10 Hz [*Irwin*, 1980; *Wu and Stathopoulos*, 1994] and has been used successfully in a variety field and wind tunnel studies with varying flow conditions and surface roughness configurations [*Irwin*, 1980; *Wu and Stathopoulos*, 1994; *Monteiro and Viegas*, 1996; *Wyatt and Nickling*, 1997; *Crawley and Nickling*, 2003]. The dynamic pressure differential is measured between two ports, one at the surface and the other at a height of 0.00175 m above the surface. The details of the calibration of the Irwin sensors and the subsequent calculation of τ_S are described in detail by Gillies et al. (submitted manuscript, 2005).

[27] Drag force on individual elements at three locations within the array and one position external to the array (i.e., upwind of the array) was measured using drag balances to which buckets were fixed (Gillies et al., submitted manuscript, 2005).

3.4. Sediment Transport

[28] A wedge-shaped sediment trap was used to capture sand moving in saltation (Figure 3a) and is similar to one described by *Nickling and McKenna Neuman* [1997]. The modified traps used in this study were designed to self-orient into the wind. As well, the sand collected in the trap was continuously weighed by an electronic balance located below the trap head that resolved the accumulating mass of sand at 1 Hz. The dimensions of the trap orifice are 0.02 m × 0.30 m, and four traps were placed near the centerline of the roughness array, with one being upwind of the array (5.27 m) and the other three spaced through the array (Table 1).

[29] Saltation activity at a point upwind of the roughness array and at three locations within the array was also monitored using four piezoelectric Safire saltation sensors [*Baas*, 2004] (Figure 3b) to compliment the trap data. The Safire has a 0.02 m wide sensitive surface around its circumference, 0.12 m from its tip. The Safire outputs a millivolt (mV) signal that increases proportionally with saltation activity. The mV signal is recorded by the data logger at a rate of ≈3 Hz. For these experiments the Safires were placed close (within several meters) to the sediment traps. They were not calibrated prior to deployment to allow estimation of a horizontal flux of sand, however they did

Table 2. Dates, Durations, and Wind Speed Conditions for the Sediment Transport Events

λ	Date	Event Duration, hours	Average Wind Direction at 9 m, deg	Average Wind Speed at 9 m, m s^{-1}	Average Shear Velocity, m s^{-1}	
					Smooth Surface	Rough Surface
0.030	23/5/2004	10	235	9.04	0.41	0.45
0.038	30/4/2004	12.5	216	10.07	0.45	0.58
0.050	01/5/2004	6.2	280	9.91	0.44	0.57
0.050	12/5/2004	9.9	230	8.85	0.40	0.51
0.050	13/5/2004	9.5	227	9.30	0.42	0.53
0.062	22/4/2004	9.0	235	9.43	0.42	0.57
0.062	23/4/2004	7.5	232	9.50	0.43	0.57

provide a complimentary method to quantify saltation activity.

4. Results

[30] During the 2004 field measurement period several sediment transport events lasting from ≈6 hours to over 12 hours were recorded for the four roughness arrays. These sampling periods were frequently characterized by intermittent sand transport. The dates of the sediment transport events for each of the roughness densities are listed in Table 2. The average 9 m wind speed and wind direction values in Table 2 are based on all the acceptable 10-min averaged data (based on 1 Hz acquisition) during the stated intervals. For transport of sand to occur, mean wind speed at 9 m had to generally exceed 8.5 m s^{-1}. On the basis of estimated aerodynamic roughness lengths presented by Gillies et al. (submitted manuscript) for these surfaces, an average threshold shear velocity can be calculated for the smooth upwind surface as well as the rough surfaces (Table 2). The u_{*tS} associated with sand entrainment and transport on the upwind surface was approximately 0.40 m s^{-1}.

[31] The intermittent nature of the sand transport and the small amounts being transported over short time intervals made it difficult to assess the dynamics of the sediment transport system. However, the amounts of accumulated sand for the entire periods of time over which transport occurred at the different measurement locations clearly demonstrate the influence of the roughness elements on the sediment transport system.

[32] To compare the relative amounts of sediment flux at each measurement location in a roughness array, the sum of the sand mass in each trap was calculated and then normalized by dividing by the total mass of sediment collected in the upwind out-of-array trap. The normalized saltation flux (NSF) was calculated for each trap for each period when sediment transport occurred.

[33] A similar procedure was also carried out for the Safire data. The saltation activity for an individual Safire was calculated by subtracting the modal millivolt (mV) value for the time series data from each individual Safire mV reading in the time series. During the intermittent transport experienced during these measurements, the modal value effectively represents the zero transport off-set mV value for a Safire. If the measured value minus the modal value was < 0 it was subsequently removed from the series. The remaining mV readings were summed and then normalized by dividing by the sum of the mV for the Safire in front of the roughness array. This provides a dimensionless measure of the saltation activity within the array at a given point compared with the activity at the same location in the absence of roughness. In this regard, the Safire data are comparable to the NSF measured with the traps.

[34] The relationship between NSF as function of normalized downwind distance (NDD) for each of the roughness arrays including both the trap and Safire data, and combining data from all measurement periods is shown in Figure 4. NDD is expressed as the ratio of the distance upwind or downwind of the leading edge of the roughness array to a sediment trap or Safire divided by the roughness element height (i.e., NDD = x/h). Distance downwind of the leading edge of the roughness is expressed as a negative value in this paper. The positions of the traps and Safires changed between the four λ configurations due to changes in row spacing, so the NDD designated positions of the instruments differ slightly between different λ (Table 1).

[35] The change in NSF as a function of NDD is well described by an exponential function of the form NSF = a $e^{(b\times NDD)}$ (Figure 4). In this function the rate of change of sediment flux as a function of downwind distance in the array is characterized by the b coefficient. The b coefficient is plotted as a function of λ in Figure 5. The relationship shown in Figure 5 suggests that λ affects the rate at which the sediment flux adjusts to the roughness configuration. The denser the roughness array, the greater is the reduction in transport as a function of NDD.

[36] At the monitoring locations farthest downwind in the roughness arrays the average percent reduction at the least dense array (λ = 0.03) is ≈64% compared with the out of array flux and ≈93% for the most dense array. This percent reduction observed at NDD ≈ −108 also scales with λ as shown in Figure 6 and is best described by a power function.

[37] Considering the intermittent nature of the fluxes, the supply limited transport conditions, and the complexities associated with the presence of roughness elements, the relationships are remarkably strong and consistent with transport data measured in much less complex situations (i.e., flat, transport limited surfaces) presented by other investigators [e.g., *Nickling and McKenna Neuman*, 1995, 1997; *McKenna Neuman*, 1998; *Al-Awahdi and Willetts*, 1999].

5. Discussion

[38] A large proportion of sediment transport studies presented in the literature deal with relatively simple systems where sediment supply is not limited (e.g., sediment transport on sand dunes and sand sheets). In many arid and semiarid environments such as those found at the Jornada

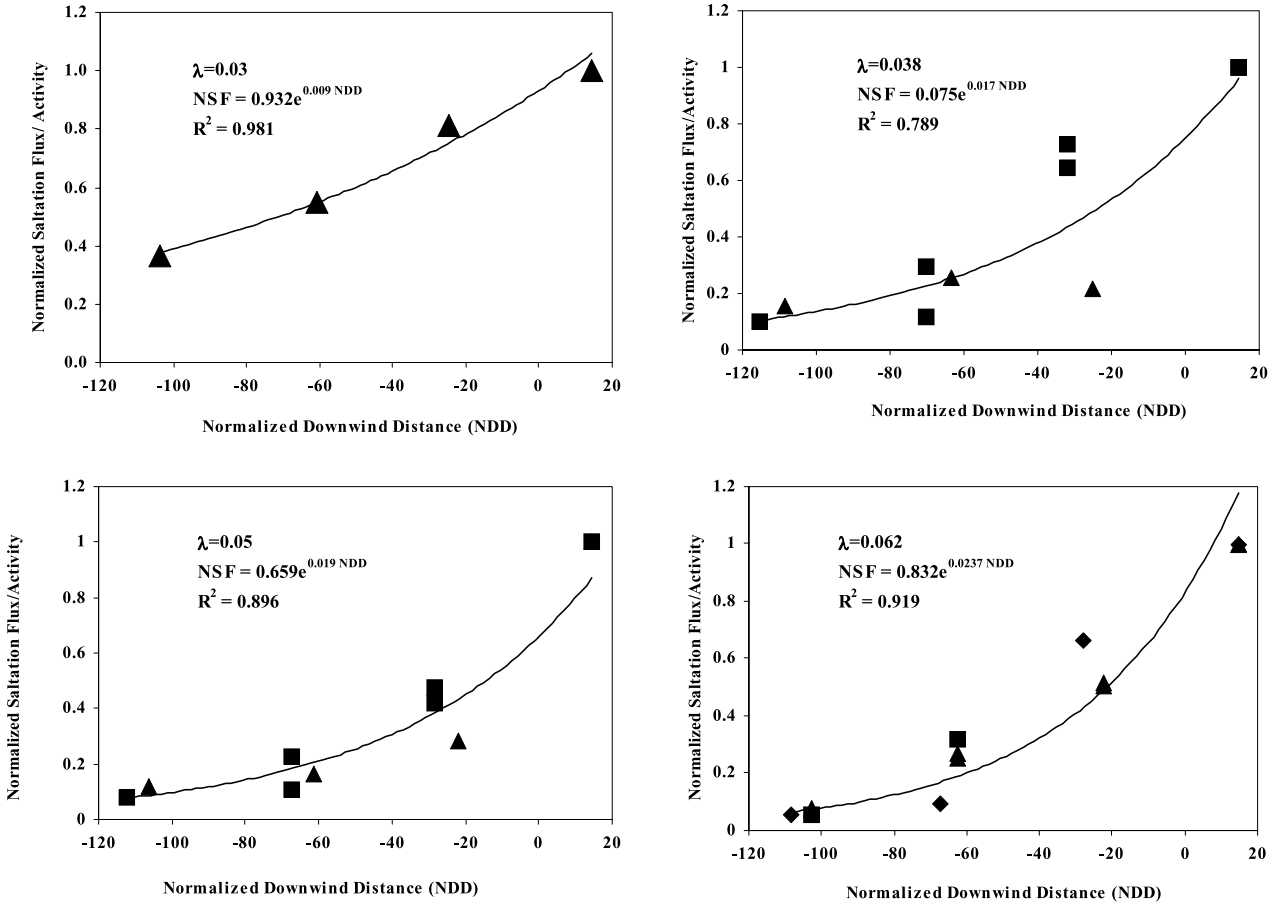

Figure 4. The relationship between NSF and NDD (i.e., NDD = x/h) for the 4 roughness arrays. Data from the traps are represented by the solid triangles and from the Safires with solid squares and solid diamonds.

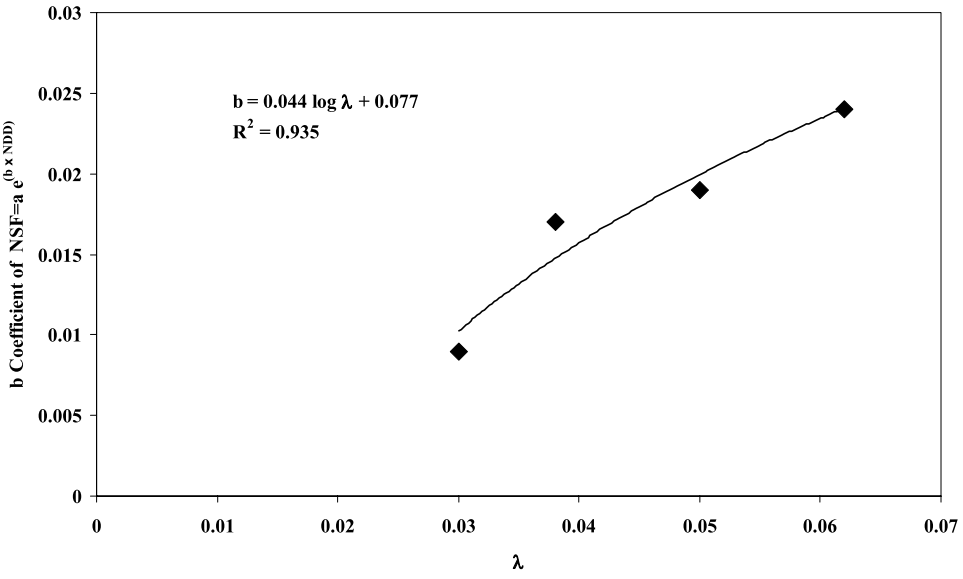

Figure 5. The relationship between the b coefficient in the NSF = a $e^{(b \times NDD)}$ relationship plotted as a function of λ, showing that the rate of change in NSF as a function of NDD is dependent on the roughness density.

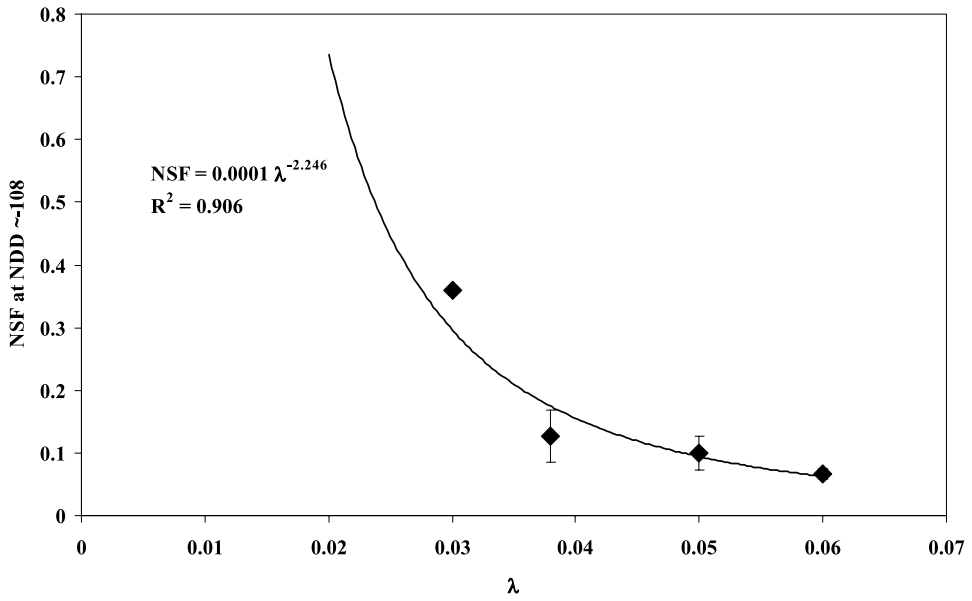

Figure 6. The relationship between average normalized saltation flux (NSF) near the downwind edge of the roughness arrays and λ.

site, the transport systems are often supply limited and characterized by intermittent sediment transport. Supply-limited transport conditions are used to describe the situation when the flux of sand is less than the transport capacity of the wind [*Gillette and Chen*, 2001]. At the Jornada Experimental Range research site, sand is entrained from a coppice dune field upwind of the roughness arrays, which stretches the entire length of the western edge of the Scrape site. The roughness array was embedded within the Scrape site. The entrained sand is transported approximately 60 m across an unobstructed, crusted surface before entering the roughness array. Once the transported sand enters the roughness arrays the horizontal flux is further modulated by the shear stress conditions within the array as well as through interactions with the roughness elements.

[39] In all four of the roughness densities tested the sediment transport rate decreases exponentially as a function of downwind distance, and this rate of change scales as a function of λ. *Lancaster and Baas* [1998] also noted a decrease in saltation flux as a function of downwind distance for wind-driven sediment transport in sparsely vegetated (*Distichlis spicata*, saltgrass) communities on sandy portions of Owens Lake, CA, although no functional relationship was defined in their study.

[40] The percent reduction in sediment transport through the arrays in the Jornada experiments can be compared with transport rate reductions due to roughness observed in other studies presented in the literature. The wind tunnel study of *Al-Awadhi and Willetts* [1999] examined the sand transport rates through surfaces that were roughened with small cylinders (diameter = 0.0023 m and h = 0.0023 m, or 0.0046 m) and configured for three roughness densities (i.e., λ = 0.046, 0.092, and 0.369). They measured the flux of sand in front of and near the trailing edge of the roughness elements with sediment traps. For the surface with λ = 0.046, which is very similar to the λ = 0.05 roughness configuration of the Jornada experiment, *Al-Awadhi and Willetts* [1999] reported NSF values of 0.86, 0.827, and 0.88. These values are directly comparable to the NSF values shown in Figure 4 for the λ = 0.05 roughness configuration. At this roughness density the saltation flux measured in the field was reduced by ≈50%, 7 m into the roughness and over 88% (NSF = 0.12) at the furthest downwind monitoring location.

[41] Figure 7 shows the relationship between NSF and λ for the *Al-Awadhi and Willetts* [1999] data and for the four Jornada roughness arrays at NDD ≈ −108, which is in this case assumed to be close to the equilibrium transport rate. The data from Jornada show a significantly greater reduction in transport rate as a function of λ than do the wind tunnel data of *Al-Awadhi and Willetts* [1999].

[42] The same comparison can be made with saltation flux measurements recorded in the presence of saltgrass elements approximately 0.10 m in height for three surfaces of different λ by *Lancaster and Baas* [1998]. From their field study, *Lancaster and Baas* [1998] present saltation flux data for a bare sand surface and three sparsely vegetated sand surfaces (λ = 0.0395, 0.0948, 0.2120) for 16 transport events, from which NSF values can be calculated. These data provide one direct comparison with the Jornada data for the λ ≈ 0.04 configuration. For this case the average NSF for the saltgrass community was 0.61 and for the equivalent Jornada λ the NSF was 0.13. Similarly to the *Al-Awadhi and Willetts* [1999] data, the Jornada transport rate was reduced in comparison to a surface with a similar λ, even though in this case both were field measurements. In all three cases however, the changes in NSF as a function of λ are well described by power functions (Figure 7). The NSF and λ relationship for the data of *Lancaster and Baas* [1998] and *Al-Awadhi and Willetts* [1999] compare very favorably with similar exponents and constants in the least squares derived regression equations (Figure 7).

[43] Several arguments can be put forth to explain the discrepancy between the Jornada data and the data of *Al-Awadhi and Willetts* [1999] and *Lancaster and Baas* [1998], which include (1) shear stress partitioning effects

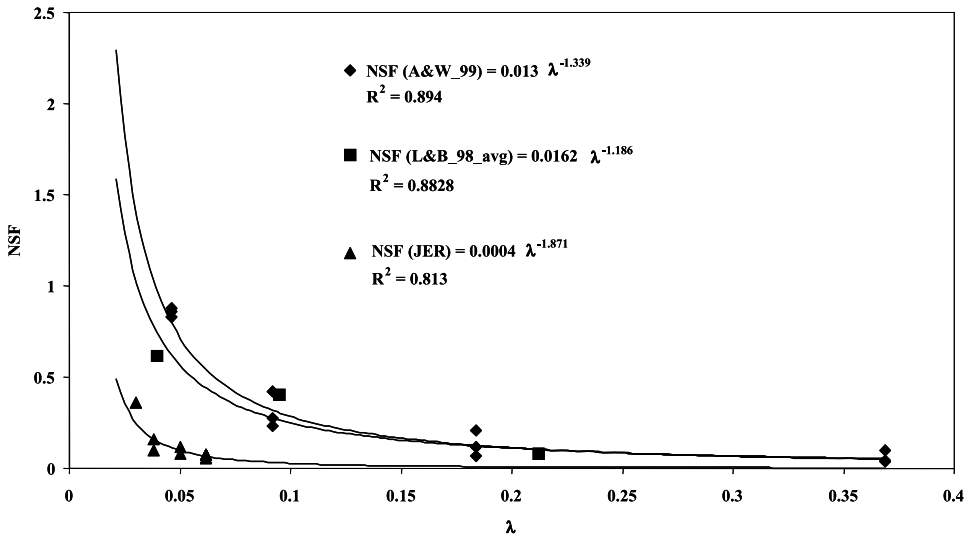

Figure 7. The relationship between NSF and λ for the data of *Al-Awadhi and Willetts* [1999] (solid diamonds), *Lancaster and Baas* [1998] (solid squares), and the Jornada experiments (solid triangles) showing that the Jornada flux rates are very much reduced compared with data for surfaces of similar roughness density.

and (2) element size effects. Each of the above arguments is addressed below in detail.

[44] Several authors have proposed simple models for the prediction of sediment transport in the presence of surface roughness based on the shear stress partitioning concepts of *Schlichting* [1936] and others. *Greeley et al.* [1995], for example, proposed a model that attempted to account for the effect of surface roughness on sediment transport based on an empirical relationship using *Marshall*'s [1971] shear stress partitioning data and *Bagnold*'s [1941] well known power relationship between u_* and Q, which they express as:

$$\frac{Q_R}{Q} = \left(\frac{1 - 3 \times (\lambda)}{1 + 1.8 \times (1 - e^{-10 \times \lambda})}\right) \tag{5}$$

where Q_R is saltation transport rate on a surface with nonerodible elements, and Q is saltation transport rate on the same surface in the absence of the nonerodible elements.

[45] *Orndorff* [1998] proposed that roughness effects on sand transport could be predicted using *Raupach et al.*'s [1993] shear stress partitioning model and *Bagnold*'s [1941] transport relationship. Once the shear stress partitioning ratio (R) for a surface is known, Q_R can be estimated from the calculated τ_S via the *Bagnold* [1941] saturated transport rate relationship:

$$Q_R = 1.5\left(\frac{D}{0.00025}\right) \times \left(\frac{\rho_p}{g}\right) \times u_{*S} \tag{6}$$

where D is grain diameter (m), g is acceleration due to gravity (m s^{-2}), ρ_p is particle density (kg m^{-3}), and u_{*S} is equal to $(\tau_S/\rho_a)^{0.5}$ (N m^{-2}).

[46] The predicted values of NSF for the *Greeley et al.* [1995] and *Orndorff* [1998] models as a function of λ are plotted in Figure 8 along with the field data from the Jornada experiment, the field data of *Lancaster and Baas* [1998], and the wind tunnel data of *Al-Awahdi and Willetts* [1999].

[47] As shown in Figure 8, *Orndorff*'s [1998] model appears to provide a relatively good fit to both the field data of *Lancaster and Baas* [1998] and the wind tunnel data of *Al-Awahdi and Willetts* [1999]. This model however, does not fit the Jornada data, which are characterized by supply limited conditions. The *Greeley et al.* [1995] model does not fit any of the measurements found in the three studies for $\lambda > 0.10$.

[48] The relationship between the normalized sediment flux and surface shear stress conditions within the different roughness arrays is shown in Figure 9. Gillies et al. (submitted manuscript) measured local average R values and normalized element drag force on the roughness elements (NED) through the length of the roughness arrays, which can be compared with the sediment flux data. As Figure 9 shows, NSF decreases as a function of NDD at a much greater rate than both R and NED. For NDD < -60, τ_S remains relatively constant in the arrays, indicating that there is similar amounts of shear stress on the surface through the rest of an array. Once a relatively constant τ_S is established in a roughness array the sediment transport rate could be expected to adjust to this new stress condition. This however was not the case as sediment was being removed from transport through the length of a roughness array.

[49] The continued decline in sediment transport rate through the roughness arrays appears to be the result of two mutually enhancing interactions between the sand in transport and the roughness elements. The first effect is the loss of sediment in zones of reduced shear behind the roughness elements. Small deposits of sand were observed near the bases of the roughness elements following the transport events. In effect, the sand available for transport decreases as a function of downwind distance through the arrays.

[50] In addition to this trapping efficiency is the effect of the nonerodible elements on the number and competence of grain/bed collisions. For small roughness elements, such as the cylinders used by *Al-Awadhi and Willetts* [1999], the

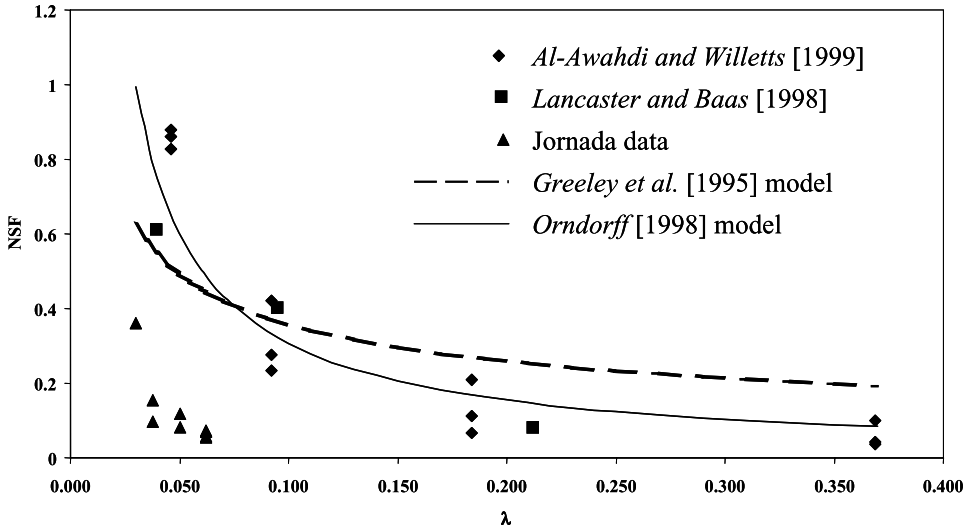

Figure 8. Comparison between the measured NSF data as a function of λ from *Al-Awadhi and Willetts* [1999], *Lancaster and Baas* [1998], and the Jornada data, and the modeled relationships proposed by *Greeley et al.* [1995] and *Orndorff* [1998].

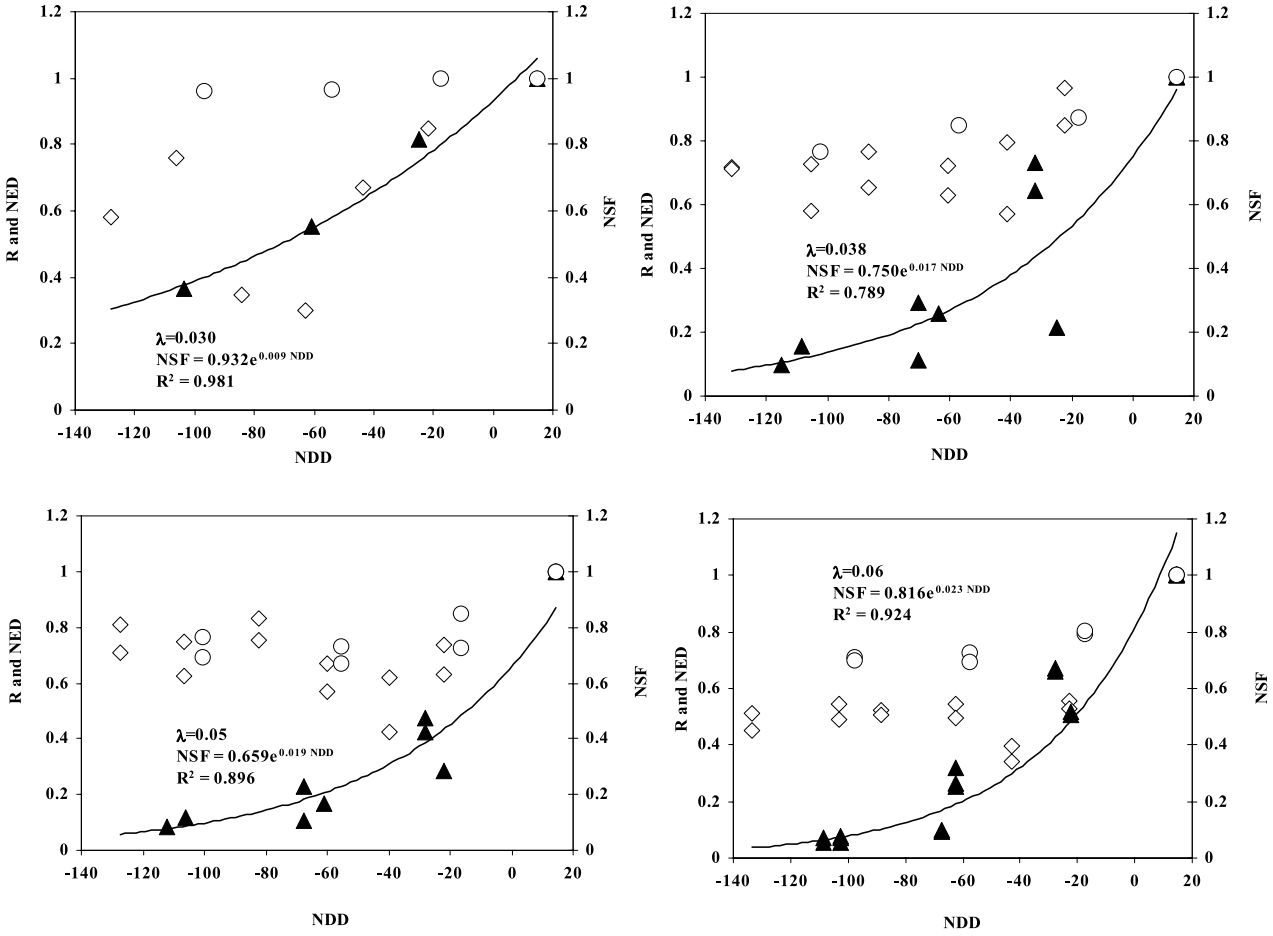

Figure 9. A comparison between the relationships between normalized saltation flux (NSF, solid triangles) and normalized downwind distance (NDD) and between normalized surface shear stress (*R*, open diamonds) and normalized element drag force (NED, open circles) and NDD for each of the four roughness densities. *R* and NED data are from Gillies et al. (submitted manuscript). The plots show that even though surface shear and element drag forces remain relatively constant for NDD < −42, there is a continued decrease in sediment transport past this point.

heights of saltation trajectories for some sand particles can far exceed the height of the roughness elements. Once above the roughness the saltating particles receive momentum from the wind, accelerate and subsequently impact the erodible surface helping to drive the saltation system, maintaining a more efficient system in the presence of small roughness elements. *Bagnold* [1941] also suggested that sand grains moving over certain types of surfaces (e.g., pebble-covered) conserves momentum because of highly elastic collisions with the roughness, resulting in the more rapid transport of the grains and the transfer of additional momentum to the surface upon impact with the intervening surface.

[51] Typically most saltating particles travel below 0.30 m with a large percentage of the grains moving between 0 and 0.10 m [*Sørensen*, 1991; *Cooke et al.*, 1993]. For the Jornada experiments the saltation trajectory heights interact with the roughness elements throughout the portion of the saltation cloud height where most of the flux occurs. The interaction between the large Jornada roughness elements and saltating sand grains creates conditions that are much more restrictive to the downwind movement of sand than for smaller elements. The ratio of saltation cloud height to roughness element height is near one (assuming a 0.30 m deep saltation cloud) for the Jornada experiments compared with 3 for the conditions measured by *Lancaster and Baas* [1998] and 8–15 for the wind tunnel study of *Al-Awadhi and Willetts* [1999].

[52] Other processes that may cause diminution of flux with downwind distance is the dispersion of the sand due to the three-dimensional character of the saltation granular splash and the variability in wind direction. This could be especially significant if the source of sand had been essentially a point source. In this field setting, however, the sand entrained from the coppice dune field moved across the entire Scrape site passing on either side of the roughness arrays. In this situation, dispersion would not likely be a dominant process causing grains to move laterally through the sides of the roughness arrays, where they would be lost from the system.

[53] A second component of roughness form may also contribute to the reduced efficiency of sediment transport in the Jornada experiment. The frontal area of these large roughness elements ($\approx$0.101 m^2) occupies considerable space across the area defined by the length of a row times the height of elements. In effect the (horizontal) porosity, defined as open area divided by total area [*Cornelis and Gabriels*, 2005] for each roughness density can be calculated. Because of the staggered array form, the open area is defined in this case as the total area minus the sum of all element frontal area in two sequential rows. For the most dense array ($\lambda = 0.062$), 30% of the unit area through which the sand is passing is occupied by solid elements, which drops to only 16% in the most open array ($\lambda = 0.03$).

[54] The exposed upwind surfaces of the roughness elements will be a zone of impact for some of the saltating grains. Particles striking the roughness elements on their windward side will rebound most often in an upwind direction, moving in opposition to the wind flow direction. This should reduce the overall the downwind flux of particles and create a population of rebounding grains with reduced energy for splashing up new grains as opposed to those moving with the wind. This condition is opposite to the *Bagnold* [1941] argument for increased momentum transfer under certain roughness conditions (i.e., small, hard, highly elastic elements). These rebounding grains may also find themselves landing in the zone of reduced shear stress created by the row of elements immediately upwind to their point of impact. These processes would appear to work in concert to deplete the sediment transport rate incrementally through the array.

[55] Both the effects of element height and width on sediment transport rates at Jornada are directly related to the similar length scales associated with the size of the elements and typical saltation length units (path lengths and trajectory heights). It is unlikely that sand flux through a roughness patch would reach zero, as long as τ_S remained above threshold, for the same reason cited by *Nickling and Mckenna Neuman* [1995], who argued that localized, spatially and temporally variable points of high instantaneous shear stress at the bed created by eddies shed from individual elements are sufficient to keep some particles in motion. In addition to these localized zones where transport can be initiated or sustained at some reduced level, it is also possible that higher-magnitude stress events (turbulent eddies) generated in the flow above the elements may on occasion reach the surface and help to sustain sediment transport.

[56] Although the sediment transport system was supply limited during the experiments described in this study, we believe that with the removal or relaxation of this limitation the results would be comparable. The processes leading to the diminution of flux through the roughness arrays that we have described will occur even in the presence of increased sediment loads. The reduction in the relative amount of sediment in transport may in fact be further reduced due to less elastic collisions between the saltating sand and a softer bed of sand, compared with the harder bounding surface at the Scrape site. However, this may be counteracted by the larger number of grains that would be set in motion by the impacting saltating grains. Further research is needed to ascertain the magnitude of the influence of sediment supply during aeolian transport occurring over rough surfaces.

6. Conclusions

[57] Results of these tests indicate that sediment transport rates through patches of roughness in the atmospheric ISL are controlled to a large extent by the roughness density of the surface. This was also illustrated by the use of data gleaned from publications by *Lancaster and Baas* [1998] and *Al-Awadhi and Willetts* [1999]. The data presented in this paper shows that knowledge of the roughness density of a surface can be used to predict the effect roughness has on reducing saltation flux compared with a similar surface in the absence of nonerodible roughness elements. However, it appears that element size plays an important role in influencing the magnitude of the reduction that cannot be accounted for based solely on knowledge of λ. This dimensionless parameter has proven to be a good descriptor of roughness to predict how the shear stress of the boundary layer will be partitioned between roughness elements and the surface, and as demonstrated by *King et al.* [2005] the *Raupach et al.* [1993] relationship holds over a wide range of element sizes.

[58] On the basis of a limited data set presented in this paper, the *Raupach et al.* [1993] shear stress partitioning model as it is incorporated into *Orndorff*'s [1998] sediment transport model, appears to work reasonably well for predicting the effect of roughness on sand transport in the cases where the roughness elements are $\leq$ 0.10 m in height (Figure 8). However, when the dimensions of the roughness itself are equivalent to the full range of saltation length units it appears that additional effects caused by the interaction of the elements with the saltation cloud reduce the transport efficiency to a much greater extent than for surfaces with smaller roughness elements of equivalent roughness density (Figure 8). This limits the applicability of the *Orndorff*'s [1998] model. On the basis of the results presented in this paper a sediment transport model that uses a shear stress partitioning approach as a framework must incorporate a scale dependency effect linked to the physical dimensions of the roughness.

[59] For terrestrial aeolian sand transport the saltation unit lengths are fairly well understood [e.g., *Anderson and Hallet*, 1986; *Shao and Li*, 1999] and the results from this study can form the basis for modifying sediment transport models that incorporate roughness effects. In applying these results and developing models for the Martian aeolian transport system, consideration must be given to the different saltation unit lengths in that environment. For Mars, with its reduced gravity and atmospheric density, the saltation path length has been estimated between 12.5 m [*Cooper and Mustard*, 1998] and 41.7 m [*Greeley and Iversen*, 1985]. Because the saltation trajectory path lengths are long, the incident angles of the impacting particles should also be lower than those on Earth [*Greeley and Iversen*, 1985]. These properties of the Martian saltation system would suggest the constraints that element size have on terrestrial saltation may be relaxed somewhat as the roughness elements on erodible surfaces on Mars are within the same size range as terrestrial roughness. The results from this work can form the basis for evaluating and modeling roughness effects on aeolian sediment transport on Mars in a shear stress partitioning framework.

Notation

b element breadth, m
d displacement height, m
D grain diameter, m
g acceleration due to gravity, m s^{-2}
h element height, m
ISL inertial sublayer
m empirical constant between 0 and 1
n number of roughness elements occupying the ground area of the roughness array
NDD normalized downwind distance, x/h, dimensionless
NSF normalized saltation flux, dimensionless
Q horizontal saltation flux on a surface without roughness elements, kg m^{-1} s^{-1}
Q_R horizontal saltation flux on a surface with nonerodible elements, kg m^{-1} s^{-1}
R shear velocity ratio, dimensionless
R_t threshold wind shear velocity ratio, dimensionless
u wind speed, m s^{-1}
u_* wind shear velocity, m s^{-1}
u_{*S} wind shear velocity based on the relationship $(\tau_S/\rho_a)^{0.5}$, m s^{-1}
u_{*tR} threshold wind shear velocity with roughness elements, m s^{-1}
u_{*tS} threshold shear velocity of bare surface, m s^{-1}
x downwind distance, m
z reference height above surface, m
z_o aerodynamic roughness length, m
β ratio of element to surface drag coefficients, dimensionless
κ von Kármán constant, 0.4
λ roughness density, dimensionless
ρ_a air density, kg m^{-3}
ρ_p particle density, kg m^{-3}
σ roughness element basal area to frontal area ratio, dimensionless
τ total surface shear stress, N m^{-2}
τ_S surface shear stress on the area not covered by the roughness elements, N m^{-2}

[60] **Acknowledgments.** This work was funded in part through the NASA, Mars Fundamental Research Program (grant NAG5-12759). W. G. Nickling also gratefully acknowledges the financial support of the Natural Sciences and Engineering Research Council of Canada (grant 7427-02). Logistical support from the USDA Jornada Experimental Range Personnel was greatly appreciated and instrumental in the success of this project. The authors would like to thank Shannon Brown and Jennifer Bryant from the University of Guelph for their assistance in instrument set-up and diligence in keeping the field site in operation. Kurt Cupp of the Desert Research Institute ably assisted in the instrument fabrication, set-up, and programming of the data acquisition systems as part of this project. Mario Finoro and Sandy McLaren of the University of Guelph also contributed to the instrument design and fabrication. Thanks finally to Torin Macpherson, Matt Alexander, Andrew Torcoletti, Jennifer Booth, and Laura Brown from the University of Guelph who participated as part of the JER field studies and to Dale and Jane Gillette for their support while at the JER. The insightful comments of the JGR editors and reviewers are also gratefully acknowledged.

References

Al-Awadhi, J. M., and B. B. Willetts (1999), Sand transport and deposition within arrays of non-erodible cylindrical elements, *Earth Surf. Processes Landforms*, *24*, 423–435.

Al-Sudairawi, M. (1992), The effect of non-erodible elements on sand transport rate, Ph.D. thesis, Univ. of Aberdeen, Aberdeen, Scotland.

Anderson, R. A., and B. Hallet (1986), Sediment transport by wind: Toward a general model, *Geol. Soc. Am. Bull.*, *97*, 523–535.

Anderson, R. S., and B. B. Willetts (1991), A review of recent progress in our understanding of aeolian sediment transport, *Acta Mech.*, *1*, 1–19.

Baas, A. (2004), Evaluation of Saltation Flux Impact Responders (Safires) for measuring instantaneous aeolian sand transport rates, *Geomorphology*, *59*(1–4), 99–118.

Bagnold, R. A. (1941), *The Physics of Blown Sand and Desert Dunes*, 265 pp., CRC Press, Boca Raton, Fla.

Buckley, R. (1987), The effect of sparse vegetation cover on the transport of dune sand by wind, *Nature*, *325*(6103), 426–428.

Cooke, R. U., A. S. Goudie, and A. Warren (1993), *Desert Geomorphology*, 526 pp., UCL Press, London.

Cooper, C. D., and J. F. Mustard (1998), Rates of erosion in Oxia Palus, Mars, *Lunar Planet. Sci. Conf. Abstr.*, *XXIX*, Abstract 1164.

Cornelis, W. M., and D. Gabriels (2005), Optimal windbreak design for wind erosion control, *J. Arid Environ.*, *61*, 315–332.

Crawley, D., and W. G. Nickling (2003), Drag partition for regularly-arrayed rough surfaces, *Boundary Layer Meteorol.*, *107*, 445–468.

Gillette, D. A., and W. Chen (2001), Particle production and aeolian transport from a "supply-limited" source area in the Chihuahuan Desert, New Mexico, United States, *J. Geophys. Res.*, *106*, 5267–5278.

Gillette, D. A., and P. H. Stockton (1989), The effect of nonerodible particles on the wind erosion of erodible surfaces, *J. Geophys. Res.*, *94*, 12,885–12,893.

Greeley, R., D. Blumberg, A. Dobrovolskis, L. Gaddis, J. D. Iversen, N. Lancaster, K. R. Rasmussen, R. S. Saunders, S. Wall, and B. R. White (1995), Potential transport of windblown sand: Influence of surface

roughness and assessment with radar data, in *Desert Aeolian Processes*, edited by V. P. Tchakerian, pp. 75–100, CRC Press, Boca Raton, Fla.
Greeley, R., and J. D. Iversen, (1985), *Wind as a Geological Process on Earth, Mars, Venus and Titan*, 333 pp., Cambridge Univ. Press, New York.
Irwin, H. P. A. H. (1980), A simple omnidirectional sensor for wind tunnel studies of pedestrian level winds, *J. Wind Eng. Ind. Aerodyn.*, *7*, 219–239.
Jackson, P. S. (1981), On the displacement height in the logarithmic velocity profile, *J. Fluid Mech.*, *111*, 15–25.
King, J., W. G. Nickling, and J. A. Gillies (2005), Representation of vegetation and other non-erodible elements in aeolian shear stress partitioning models for predicting transport threshold, *J. Geophys. Res.*, *110*, F04015, doi:10.1029/2004JF000281.
Lancaster, N., and A. Baas (1998), Influence of vegetation cover on sand transport by wind: Field studies at Owens Lake California, *Earth Surf. Processes Landforms*, *25*, 68–82.
Logie, M. (1981), Wind tunnel experiments on dune sands, *Earth Surf. Processes Landforms*, *6*, 365–374.
Lyles, L., R. L. Schrandt, and N. F. Schneidler (1974), How aerodynamic roughness elements control sand movement, *Trans. ASAE*, *17*, 134–139.
MacDonald, R. W., R. F. Griffiths, and D. J. Hall (1998), An improved method for the estimation of surface roughness of obstacle arrays, *Atmos. Environ.*, *32*(11), 1857–1864.
Malin, M. C., et al. (1998), Early views of the Martian surface from the Mars Orbiter Camera of Mars Global Surveyor, *Science*, *279*(5357), 1681–1685.
Marshall, J. K. (1971), Drag measurements in roughness arrays of varying density and distribution, *Agric. Meteorol.*, *8*, 269–292.
McEwan, I. K., and B. B. Willetts (1994), On the prediction of the bedload sand transport rate in air, *Sedimentology*, *41*(6), 1241–1251.
McKenna Neuman, C. (1998), Sediment flux and boundary layer adjustments over rough surfaces with an unrestricted, upwind sediment supply, *Geomorphology*, *25*, 1–17.
McKenna Neuman, C. L., and W. G. Nickling (1995), Aeolian sediment flux decay: Non-linear behaviour on developing deflation lag surfaces, *Earth Surf. Processes Landforms*, *20*, 423–435.
Monteiro, J. P., and D. X. Viegas (1996), On the use of Irwin and Preston wall shear stress probes in turbulent incompressible flows with pressure gradients, *J. Wind Eng. Ind. Aerodyn.*, *64*, 15–29.
Nickling, W. G., and C. McKenna Neuman (1995), Development of deflation lag surfaces, *Sedimentology*, *42*(3), 403–414.
Nickling, W. G., and C. McKenna Neuman (1997), Wind tunnel evaluation of a wedge-shaped aeolian transport trap, *Geomorphology*, *18*, 333–345.
Orndorff, R. (1998), A stochastic model of wind-induced shear stress partitioning between an erodible soil surface and roughness elements, in *Dust Aerosols, Loess Soils and Global Changes*, edited by A. J. Busacca, pp. 75–78, Wash. State Univ. Coll. Agric. and Home Econ., Pullman.
Raupach, M. R. (1992), Drag and drag partition on rough surfaces, *Boundary Layer Meteorol.*, *60*, 375–395.
Raupach, M. R., D. A. Gillette, and J. F. Leys (1993), The effect of roughness elements on wind erosion threshold, *J. Geophys. Res.*, *98*, 3023–3029.
Schlichting, H. (1936), Experimentelle untersuchungen zum rauhigkeitsproblem, *Ing. Arch.*, *7*, 1–34.
Shao, Y., and A. Li (1999), Numerical modelling of saltation in the atmospheric surface layer, *Boundary Layer Meteorol.*, *91*(2), 199–225.
Sørensen, M. (1991), Estimation of some aeolian saltation transport parameters from transport rate profiles, *Acta Mech.*, *1*, 141–190.
Sørensen, M. (2004), On the rate of aeolian sand transport, *Geomorphology*, *59*, 53–62.
White, B. R., and H. Mounla (1991), An experimental study of Froude number effect on wind-tunnel saltation, *Acta Mech. Suppl.*, *1*, 145–157.
Wilson, S. A., and J. R. Zimbelman (2004), Latitude-dependent nature and physical characteristics of transverse aeolian ridges on Mars, *J. Geophys. Res.*, *109*, E10003, doi:10.1029/2004JE002247.
Wooding, R. A., E. F. Bradley, and J. K. Marshall (1973), Drag due to regular arrays of roughness elements of varying geometry, *Boundary Layer Meteorol.*, *5*, 285–308.
Wu, H., and T. Stathopoulos (1994), Further experiments on Irwin's surface wind sensor, *J. Wind Eng. Ind. Aerodyn.*, *53*, 441–452.
Wyatt, V., and W. G. Nickling (1997), Drag and shear stress partitioning in sparse desert creosote communities, *Can. J. Earth Sci.*, *34*, 1486–1498.

J. A. Gillies, Particle Emissions Measurement Laboratory, Division of Atmospheric Sciences, Desert Research Institute, 2215 Raggio Parkway, Reno, NV 89512, USA. (jackg@dri.edu)

J. King and W. G. Nickling, Wind Erosion Laboratory, Department of Geography, University of Guelph, Guelph, ON, Canada N1G 2W1.